Paper:
Mani Krishna, K., Leo Prakash, D., Srivastava, D., Saibaba, N., Quinta da Fonseca, J., Dey, G. & Preuss, M. (2015). Influence of Sn on Deformation Mechanisms During Room Temperature Compression of Binary Zr–Sn Alloys. *Zirconium in the Nuclear Industry: 17th Volume*, 138-158.
http://dx.doi.org/10.1520/STP154320130044

Selected Technical Papers

Influence of Sn on deformation mechanisms during room temperature compression of binary Zr-Sn alloys

Journal:	*STP: Selected Technical Papers*
Manuscript ID:	Draft
Manuscript Type:	Full Length Paper
Date Submitted by the Author:	n/a
Complete List of Authors:	Krishna, K V Mani; Material Science Division, Bhabha Atomic Research Centre, Department of Atomic Energy D, Leo Prakash; University Of Manchester, School of Materials Srivastava, D; Material Science Division, Bhabha Atomic Research Centre, Department of Atomic Energy Saibaba, Nudurupati; Nuclear Fuel Complex, Department of Atomic Energy Quinta da Fonseca, Joao; University of Manchester, School of Materials Dey, G; Material Science Division, Bhabha Atomic Research Centre, Department of Atomic Energy Preuss, Michael; The University of Manchester, School of Materials
Keywords:	Zr-Sn alloys, deformation mechanisms, intergranual strains, twinning, in-situ loading and neutron diffraction
ASTM Committees and Subcommittees:	B10.02 Zirconium and Hafnium < B10 Committee on Reactive and Refractory Metals and Alloys, B10 Committee on Reactive and Refractory Metals and Alloys
Abstract:	Role of Sn on the deformation mechanisms of Zr was investigated using in situ neutron diffraction and complementary electron microscopy techniques. Binary Zr-Sn alloys having fully recrystallized microstructure and typical rolling texture were subjected to in situ loading and diffraction experiments along the rolling direction of the sample. Significant twinning activity was observed and the twins were observed to be $\{10\bar{1}2\}\langle10\bar{1}1\rangle$ type tensile twins. Critical stress for the twin nucleation and the extent of twinning were found to be strongly influenced by the Sn content. Critical plastic strain for the nucleation of twining, however, was observed to be weakly dependent on the Sn content. Results indicate significant plastic slip activity to be a necessary condition for the onset of twinning.

SCHOLARONE™ Manuscripts

Influence of Sn on deformation mechanisms during room temperature compression of binary Zr-Sn alloys

K. V. Mani Krishna[1], D. G. Leo Prakash[2], D. Srivastava[1], N. Saibaba[3], J. Quinta da Fonseca[1], G. K. Dey[1], M. Preuss[2]

[1]Materials Science Division, Bhabha Atomic Research centre, Trombay, Mumbai, India

[2] Manchester Materials Science Centre, The University of Manchester, Grosvenor Street, Manchester M1 7HS, UK

[3]Nuclear Fuel Complex, Hyderabad, India

Abstract

Role of Sn on the deformation mechanisms of Zr was investigated using in situ neutron diffraction and complementary electron microscopy techniques. Binary Zr-Sn alloys having fully recrystallized microstructure and typical rolling texture were subjected to in situ loading and diffraction experiments along the rolling direction of the sample. Significant twinning activity was observed and the twins were observed to be $\{10\bar{1}2\}\langle 10\bar{1}1\rangle$ type tensile twins. Critical stress for the twin nucleation and the extent of twinning were found to be strongly influenced by the Sn content. Critical plastic strain for the nucleation of twining, however, was observed to be weakly dependent on the Sn content. Results indicate significant plastic slip activity to be a necessary condition for the onset of twinning.

KEYWORDS: Zr-Sn alloys, deformation mechanisms, intergranular strains, twinning, in-situ loading and neutron diffraction

Introduction

The wide spread use of Zr based structural materials in thermal nuclear reactors arises from their unique combination of resistance to environmental degradation (in the form of corrosion and mechanical degradation) combined with their high transparency to thermal neutrons [1]. One of the key alloying elements in many commercial Zr-alloys, such as Zircaloy-2, Zircaloy-4, E635 and ZIRLO™, is Tin (Sn), which was originally added to mitigate issues related to nitrogen embrittlement and to provide sufficient mechanical strength through solid solution strengthening [2,3]. However, efforts in further improving corrosion resistance of Zr cladding material have resulted in alloys with significantly reduced Sn levels. For instance, Zircaloy-4 with improved corrosion resistance was developed by reducing the Sn content. A similar trend has been pursued for ZIRLO™ and other alloys such as M5™ which do not contain any Sn [4-11]. Although there exists a rich literature on the role of Sn on corrosion behaviour of Zr based alloys [1], very limited information, if any, is available in the open literature on the role of Sn on the deformation mechanisms in such materials. In the light of aforementioned efforts to improve corrosion resistance by the reduction of the amount of Sn in Zr alloys, understanding the associated affects brought in by the changes in Sn content on the deformation behaviour of the alloy becomes pertinent. Since Zr based components are fabricated through a series of thermo mechanical treatments, involving considerable degree of deformation, a thorough knowledge of the operative deformation modes and the changes in them, if any, as a function of Sn content becomes imperative for the effective optimization of the fabrication procedures. Such knowledge is crucial for the prediction of the evolution of microstructure and texture, which in turn helps developing components with superior in-service performance.

Tin, unlike a majority of other common alloying elements used in nuclear grade Zirconium alloys (such as Fe, Cr, Nb etc) shows relatively high solid solubility and thus contributes to appreciable solid solution strengthening [12-14]. Hence, Sn has the potential of having a direct effect on the numerous possible slip systems in Zr. Deformation by slip in materials with an hcp crystal structure, such as Zr and Ti, is complicated by having easy <a> type slip modes and more difficult to activate slip modes that includes a <c> component, i.e. <c+a> slip [2,15-19]. Further, due to the difficulty of activating <c+a> slip, Zr has a significant tendency for twinning, which plays a major role in evolution of crystallographic texture of the material [15]. However, existing information on how this twinning tendency in Zr is influenced by alloying elements in general and by the Sn in particular is rather limited, forming the motivation to the present study. A particular focus of the present work is the way Sn might affect twin nucleation and overall twin activity during the early stages of deformation. It is worth mentioning here that twin nucleation criteria in materials with an hcp crystal structure are still largely unknown. While in some cases a simple stress criterion is assumed [20, 21], similar to a critical resolved shear stress for slip, there is plenty of evidence that partial dislocations are an additional requirement for twin nucleation [22, 23].

A majority of the previous deformation studies relied on the slip trace analysis of the single crystals for the study of the deformation behaviour and identification of the active slip modes [17- 19]. However, the behaviour of the polycrystalline aggregate (which is of more practical importance from the industrial application point of view) is known to be far different from that of the single crystal under similar loading conditions. Another approach was to apply

TEM (Transmission electron microscopy) based analysis on the deformed samples [16, 24]. By characterizing the dislocation structures one can identify the active deformation modes. However, this technique suffers from poor statistics, can only be used in crystals with low dislocation densities and cannot be used to derive the CRSS of the different slip systems. An elegant alternative to overcome the above mentioned limitations is to use in situ neutron diffraction during mechanical loading experiments, which acts as an efficient tool for recording the development of intergranular strains of various grain families [25- 33]. Such intergranular strain development can be seen as the fingerprint of certain deformation modes. Because of the highly penetrating nature of the neutrons, a large volume of the sample can be probed, making the measurements statistically reliable. The present study uses in situ neutron diffraction extensively along with complementary microstructural characterization tools of EBSD (Electron back scattered diffraction) and TEM to evaluate the role of Sn on the deformation modes of Zr.

Experimental

Material and processing of samples

In order to study the role of Sn on the deformation mechanisms in Zr, four model Zr-Sn binary alloys were prepared with nominal compositions of 0.15%, 0.23%, 0.33%, and 1.20% Sn (amounts are in weight percentage), balance being Zr. In order to keep the effects of the other trace elements to bear minimum, alloys were prepared from the same relatively pure nuclear grade Zr sponge. The alloy samples were prepared by quadruple electron beam melting. The cast structure of the ingots was broken by hot extrusion at 800^{o}C. Blocks of 35mm x 22 mm x 15 mm were cut from the extruded material and β heat treated at 1050°C for 20 minutes followed by water quenching. The purpose of the heat treatment was to reduce any potential microsegregation of Sn and generate a similar starting microstructure with no preferred crystallographic texture. After β quenching, the blocks were stress relieved at 500^{o}C for 24 hours followed by 1^{o}C/min cooling. Prior to hot rolling, the blocks were homogenized at 550^{o}C for 40min and subsequently rolled at 550°C to a reduction of 65% followed by annealing treatment at 550^{o}C for 24 hours. The purpose of this thermomechanical process was to generate a fully recrystallized microstructure and a typical crystallographic texture with the majority of basal poles aligned along ND (normal direction) with some spread along TD (transverse direction). The purpose of creating this microstructure was to enable compression tests with the majority of the <c> axis either aligned perpendicular (compression along RD) or nearly parallel (compression along ND) to the loading direction during the in-situ neutron diffraction studies. To date, only data from loading along RD have been fully analysed and is presented here. The samples for the in-situ compression experiments were machined to cylindrical shape with a diameter of 6mm and a length of 10mm (along the rolling direction).

In-situ loading and neutron diffraction experiments

The time of flight neutron diffracton beamline ENGIN-X, at ISIS, Rutherford Appleton laboratory, UK, was used for the in-situ compression loading and diffraction experiments for the present study [34-36]. The schematic of the experimental set up (Fig. 1), shows that the location of the detectors allows the capturing of the diffraction data along two principle directions of the sample, *e.g.,* along the rolling direction (longitudinal detector) and normal direction (transverse detector). The diffraction peaks recorded carry information regarding the lattice strain evolutions, and deformation mechanisms through the changes in their peak positions (for intergranular elastic lattice strains), intensity (for twinning) and FWHM (full width at half maximum). For instance, onset of twinning can be detected by the sudden change in the lattice strain evolutions of the grain family undergoing twinning (as shall be demonstrated in the following section). Similarly, significant changes in the FWHM of the diffraction spectra indicate towards high slip assisted plastic deformation activity from the grain families corresponding to the respective diffraction peaks.

In situ compression loading experiments were carried out using a 100 kN Instron® compression rig. The samples were compressed along the rolling direction and the data points in the elastic regime (up to ~50MPa below the macroscopic yield point) were captured in constant stress state. This is followed by a continuous strain controlled loading up to 0.18 true strain. In order to make effective use of beam time, the data points in the plastic regime were captured at two different strain rates: a slower rate of $7 \times 10^{-6}/\mathrm{s}$ until 0.025 strain followed by $2.8 \times 10^{-5}/\mathrm{s}$ until 0.18 strain. The frequency of measurement points was increased around the yield point by the deliberate selection of low strain rate, as the onset of plasticity is a key area of interest in understanding deformation mechanisms. In order to get a reasonably good signal to noise ratio of the diffraction peaks, acquisition time for the diffraction spectra at each of the measurement points was kept around 5 min, the time required to accumulate the beam current 6μA.

Microstructural characterization

Both undeformed and deformed samples were subjected to a detailed microstructural characterization using EBSD, and TEM. Sample preparation for EBSD consisted of standard metallographic preparation followed by electropolishing at 15V and a temperature of 5^{o}C in an electrolyte of 80% Methanol + 20% Perchloric acid. TEM samples were also prepared using same electrolyte in a twin jet electrolytic polisher at -40^{o}C. The EBSD analysis was carried out on the FEI Sirion FEGSEM equipped with an HKL system. For texture analysis low spatial resolution (step size of 50μm) large area maps were recorded covering an area of 70 mm^2. Microstructural orientation maps were recorded using a step size of 0.3μm covering 500 μm by 200 μm. Selected samples, subjected to low deformation levels (0.02-0.03 true strain), were examined in a JEOL 2000FX TEM for the characterization of early stages of twin formation and dislocation structure.

Results

Starting microstructure and texture

Fig. 2. depicts the typical microstructure and texture of the recrystallised material (here Zr-1.2%Sn) prior to in situ loading and diffraction experiments. No significant microstructural differences were observed in the four alloys considered for the present work. As it can be observed from the figure, the starting microstructure is completely recrystallized with an average grain size of 4.5μm (based on EBSD measurements). Grain size analysis of the other three alloys gave 5.5μm for Zr-0.15%Sn, 4.5μm for Zr-0.23%Sn and 5μm for Zr-0.33%Sn. TEM micrographs (Fig. 2.b) also show grains with low dislocation density and well defined high angle grain boundaries, typical of recrystallized material. As illustrated in the Fig. 1.c, the starting texture is predominantly basal poles aligned towards ND of the sample, with a $\sim\pm30^{o}$ spread along TD. Further, there is also a slightly preferred alignment of the $11\bar{2}0$ poles towards RD.

Macroscopic stress strain behaviour

The macroscopic stress strain behaviour of the four Zr-Sn alloys recorded during the in-situ compressive loading experiments along the rolling direction is presented in Fig. 3. As expected, with increasing Sn content the stress-strain curves exhibited higher flow stress values. The yield point data can also be found in Table 1. In addition, closer examination of the flow curves reveals the following observations:

1. The curves exhibited a comparatively flat stress-strain response regime (*i.e.*, region of low strain hardening) during the initial stage of plastic deformation, highlighted by a circle in the Fig. 3. Such flat response was more prominent with increasing Sn content.
2. The strain hardening rate in the high plastic strain domain (highlighted by rectangle), increases with Sn content.

Both observations suggest that Sn does have an effect on deformation mechanisms in these alloys.

Evolution of intergranular elastic strains as a function of Sn

For further insights into the active deformation modes and the effect of changing Sn content, we resort to analysis of the intergranular strain evolutions determined by neutron diffraction during in-situ loading. It is to be noted that the intergranular strains presented in this study do not represent the absolute elastic strain, but the relative change in strains from the unloaded condition. As described earlier, during the loading experiment the diffraction signal is recorded in the rolling (longitudinal detector) and normal (transverse detector) direction. Fig. 4, shows the evolution of the compressive elastic strain measured in the rolling (longitudinal) direction as a function of the applied stress for different grain families of the four alloys considered in the present study. In other words, we can see the elastic strain development of the grains that contribute to 0002, $10\bar{1}0$ and $10\bar{1}1$ reflections along the loading direction. During the initial stage of loading, *i.e.,* prior to the onset of plasticity, all three grain families display a reasonably linear elastic strain response. The data become particularly interesting in the moment of plasticity and the following important observations can be made.

1. The $10\bar{1}0$ grain family shows the highest degree of unloading (*i.e.,* no further increase in elastic strain despite a further increase of applied stress), which is a signature of

extensive plasticity in this grain family. It is also noticeable that the initial degree of unloading increases with increasing Sn content.

2. The extent of unloading of the $10\bar{1}1$ grain family is lower than that of the $10\bar{1}0$ grain family. However, this difference in the extent of unloading (in other words separation between the $10\bar{1}1$ and $10\bar{1}0$ responses) systematically drops with increase in Sn content.
3. The 0002 grain family exhibits significant build up of the lattice strain before a sudden unload followed by a continued increase in build up of lattice strain. As discussed in the next section, this unloading can be related to $\{10\bar{1}2\}\langle 10\bar{1}1\rangle$ tensile twinning. This twinning mode rotates the <c> axis by about 85°from the normal to rolling direction. Therefore, after the onset of twinning, the 0002 grain family detected along RD is made up of both pre existing 0002 grains and the reoriented 0002 twinned volumes. The observed unloading is a result of relatively lower elastic strain in the grains containing the twinned volumes.
4. The stress at which the onset of twinning was observed (indicated with a horizontal line in the Fig. 4) was found to increase with increasing Sn content.

Fig. 5 presents the evolution of the lattice strains recorded along the normal direction for the 0002 grain family for the Zr-0.15%Sn and the Zr-1.2%Sn alloy. This grain family is expected to display tensile twinning, moving some of the diffracting volume from normal to the rolling direction. Therefore, monitoring the 0002 reflection along ND (transverse to the loading direction) enables one to determine the intergranular strain at which twin nucleation starts. Fig. 5 demonstrates that the critical elastic strain at which twinning gets initiated is higher in the alloy with a high Sn content compared to the alloy with a low Sn content. The critical lattice strains for the onset of the twinning for all the four samples are compiled in the Table 1, which brings out the correlation between Sn content and critical lattice strain for twin nucleation.

Evolution of integrated intensity of the 0002 *reflection during loading*

Since twinning is associated with a rotation of the crystal structure, significant peak intensity variations of 0002 reflection in the measured directions (rolling and normal) can be observed during plastic deformation. In the present case, tensile twinning results in an increase in integrated intensity of the 0002 reflection with straining as shown in Fig. 6. When the change of 0002 integrated intensity is plotted against true strain, Fig.6a, it can be seen that twinning initiates between 1.3×10^{-2} and 2.1×10^{-2}. The data suggest that a slightly higher strain is required for the activation of twinning with higher Sn content, see table 1. This is consistent with the higher value of intergranular strains measured at twinning for the alloys with more Sn. The observed increase in critical strain values for the onset of twining, when viewed in the context of the expected error in the strain measurement (due to machine compliance and diffraction data being collected in continuous strain mode), suggests that critical strain changes only modestly with Sn content, unlike the critical applied stress which was found to increase significantly with the Sn content (fig 6.b and table 1). In general, twinning activity started in all of the samples between a strain of 1×10^{-2} and 2×10^{-2}. Since the actual intensity of the peak corresponds to the volume fraction of the orientations favourable for diffraction and the 0002 intensity increase in present case is due to twinning activity, one can easily infer that samples with higher Sn content exhibit higher twinning activity. When plotted against applied stress, it becomes apparent that the critical stress required for the onset of twinning is strongly dependent on the Sn content, Fig. 6.b. Table 1 provides a more quantitative picture of these observations.

Microstructure of deformed samples

In order to confirm the nature of the twins formed, and estimate their volume fraction, extensive EBSD and TEM was carried out on the deformed samples. Samples deformed in-situ in ENGIN-X were used for the purpose of EBSD characterization. An orientation map of Zr-1.2%Sn deformed to a strain of 0.18 is presented in Fig.7a demonstrating a significant presence of twins. It should be noted that this map only represents a small crop of the area scanned by EBSD. Fig. 7b highlights >15° misoriented boundaries in grey and all twin boundaries associated with $\{10\bar{1}2\}\langle 10\bar{1}1\rangle$ tensile twinning in black, which shows that the twins observed in Fig.7a are indeed of the common tensile twin type. Similar observations have been reported previously [32] for a similar starting texture and loading direction arrangement. Since the initial texture of the sample is such that majority of the basal poles are along ND and compressive loading was applied to act along RD, a majority of the grains will have their <c> axis under tension leading to the formation of tensile twins.

TEM examination was also carried out for the characterization of the twins, but on samples deformed to a plastic strain of 2-3%, with an objective of understanding the nucleation stage of twins. This strain, as can be seen in the Fig. 6a and Table 1, is just sufficient to nucleate the twins in different alloys. As shown in the Fig 8a, twins of approximately 200nm width were formed at this level of deformation. More interestingly, it was observed that, the grains in which twins could be observed have shown comparatively high dislocation density, indicating significant plasticity by slip.

Fig. 9, shows the twinning volume fraction as a function of the Sn content for the samples deformed to 0.18 compressive strain measured by EBSD. Despite the scatter of the data related to the comparatively small volume studied by EBSD, it is evident that an increase in Sn content results in an increase in twin volume fraction. This observation is in excellent agreement with the neutron diffraction observations.

Discussion

The key findings of the present study with respect to the role of the Sn on the deformation behaviour can be summarized in the following way.

- An anomalous flat response in stress-strain behaviour was observed during the initial part of plastic deformation, the extent of which increased with the Sn content.
- Initial unloading of the intergranular strains of the $10\bar{1}0$ grain family increases with rising Sn content.
- Critical macroscopic strain for the nucleation of twinning was observed to be a weak function of alloy Sn .
- Critical intergranular elastic strain and macroscopic stress for the nucleation of the twins increased significantly with increasing Sn content of the alloy.
- The extent of twinning activity increased with Sn content.

An anomalous flat response of the macroscopic stress-strain curve during the initial part of the plastic deformation has been observed by previous researchers and was attributed to thermal intergranular stresses [33, 37, 38], which are a result of the anisotropic thermal expansion coefficient for <a> and <c> direction [39]. Hence, at room temperature the <c> axis is tensioned while the <a> axis is compressed [33, 37, 38, 40]. The present work clearly shows that the degree of initial flat response depends on the level of Sn in the alloy. Therefore it seems unlikely that the thermal intergranular stresses are indeed the cause . It is very notable that during the flat response the intergranular strain increases very dramatically indicating very significant plasticity activity. However, activation of $\{10\bar{1}2\}\langle 10\bar{1}1\rangle$ tensile twinning only occurs once the flat response is overcome. EBSD and TEM analysis did not indicate any other twin activity and therefore one might argue that the flat strain response must be related to a slip burst (though strangely not resulting in any strain hardening). In fact there is a decrease in the $10\bar{1}0$ elastic strains, indicating strain softening. It appears that when the yield point of the material increases, due to solute solution strengthening of Sn, the initial strain burst also becomes more pronounced. It is likely therefore that this strain burst is related to the pinning effects of Sn. Like carbon in steels, this initial yielding seems to be discontinuous, as new dislocations are unpinned and therefore can move at a stress lower than the initial slip resistance.

The fact that increasing levels of critical plastic strain and increased critical applied stress for nucleation of twins was observed for the alloys of increasing Sn suggests that a certain amount of plastic deformation is necessary before twinning occurs in these alloys. This could be because either a there is a minimum dislocation density required for twinning to occur or that there is a need for the development of intergranular strains in the parent grains before twinning starts.

Several previous studies have indicated that availability of twinning dislocations is necessary for twin nucleation [22, 23]. Hence, the nucleation probability of twins can be thought to be proportional to the density of twinning dislocations, which in turn are proportional to the extent of the plastic activity. Present results suggest that at a strain between 1 and 2%, a sufficient density of dislocations is produced, giving rise to observed twin nucleation. Furthermore, the increased extent of unloading of the $10\bar{1}0$ grain family (see Fig. 4.) with higher Sn content indicates increased plastic activity of the twinning grain family. Therefore one might assume a rise in dislocation density with increasing Sn content at a given macroscopic plastic strain. This should in principle result in more nucleation sites for twins. In order to further support this, peak broadening (related to dislocation density) was investigated of the twin prone grain family. In principle, grains that have the normal of either their first order or second order prismatic plane aligned with the loading directions are the grains, which will twin, since their <c> axis is in the transverse orientation. Fig. 10 plots the change of FWHM of the $11\bar{2}0$ (*i.e.*, first order prismatic) reflection measured in the loading direction for Zr-0.5%Sn and Zr-1.2%Sn. It can be clearly seen that there is considerably more peak broadening in the case of Zr-1.2%Sn compared to Zr-0.15%Sn suggesting higher slip activity in case of the higher Sn containing alloy.

The other aspect is that Sn is a solid solution strengthening element in Zr alloys [41, 42] and therefore the stresses for the onset of plasticity increases with higher Sn content. Hence, the critical macroscopic stress (Fig. 6b) for twin nucleation increases. This means that a higher applied stress is required for a given plastic strain. If some amount of plastic strain is required for twin nucleation and this happens at a higher applied stress with a higher Sn content, the stress at which twinning starts is higher and therefore the twinning volume fraction will increase more rapidly. This will be enhanced by the burst like deformation caused by Sn pinning of dislocations, which also increases with Sn content.
In any case, the results suggests that increasing Sn content makes twinning nucleation happen later, that is at higher stresses and strains, but that, once it starts, it occurs more rapidly. This suggests that the major effect of Sn content on twinning is to make slip harder.

Conclusions

Present study made an extensive use of in situ neutron diffraction and complementary microstructural characterization techniques to bring out the role of Sn on the deformation behaviour of Zr. The influence of Sn on the twinning, in particular, has been quantified in terms of the critical stresses and strains required for the onset of the twins in Zr-Sn binary system. Following conclusions can be drawn from the present study.

- Sn content has been observed to have a significant effect on the activation and extent of different deformation modes of Zr, as revealed by the unloading of the various grain families during the in situ compressive deformation and diffraction experiments.
- The critical macroscopic stress and intergranual elastic strain required for twin nucleation were observed to increase with Sn content.
- A critical plastic strain is needed for the onset of the twinning in all alloys. This was found to be between 1-2%.
- The extent of twinning, defined as the twinned volume fraction after a strain of 0.18, increased with increasing Sn content.

Therefore, it appears that Sn content affects twinning simply by making deformation by slip more difficult. It makes twinning nucleation more difficult but enhances the twinning rate once twinning does start.

Acknowledgments

Present work is funded jointly by EPSRC, UK (EP/I012346/1) and Department of Atomic Energy, India, under Indo-UK collaborative programme on "Peaceful uses of Nuclear Energy".

References

[1] Cox, B., "Some thoughts on the mechanisms of in-reactor corrosion of zirconium alloys", *J. Nucl. Mater.*, Vol. 336, 2005, pp. 331–368.

[2] Linga Murty, K. and Indrajit Charit, "Texture development and anisotropic deformation of zircaloys", *Progress in Nuclear Energy,* Vol. 48, 2006, pp. 325–359.

[3] Krishnan, R. and Asundi, M. K., " Zirconium alloys in nuclear technology", *Sadhana (Indian Academy of Science Proceedings in Engineering Sciences)*, Vol. 4 (1), 1981, pp. 41-56.

[4] "Waterside Corrosion of Zirconium Alloys in Nuclear Power Plants", IAEA-TECDOC-996, 1998.

[5] Seibold, A. and Woods, K. N , "Advanced PWR cladding", *Proc of the Int Topical Mtg on Light Water Reactor Fuel Performance*, West Palm Beach, American Nuclear Soc , La Grange Park, ILL , 1994, pp. 633-642.

[6] Garzarolli, F., Broy, Y. and Busch, R. A., "Comparison of the long time corrosion behaviour of certain zirconium alloys in PWR, BWR and laboratory tests", *ASTMSTP- 1295*, 1996, pp. 850-863.

[7] Fuchs, H. P., Garzarolli, F., Weidinger, H. G., Boomer, R. P., Meier, G., Besch, O-A and Lisdat, R., "Cladding and structural material development for the advanced Siemens PWR fuel performance", *Fuel for the 90's, Proc Int Topical meeting on LWR Fuel Performance, Avignon, France, American Nuclear Society/European Nuclear Society*, 1991, pp. 682-690.

[8] Takeshi, I. and Masuto, Y., "Development of highly corrosion resistant Zirconium-base alloys", *ZR-ASTM-STP-1132*, 1991, pp. 346-367.

[9] Charquet, D., "Improvement of the uniform corrosion resistance of Zircaloy-4 in the absence of irradiation", *J. Nucl. Mater.*, Vol. 160, 1988, pp. 186-195.

[10] Doriot, S. Gilbon, Bechade,D., Mathon, J.-L., Legras,M.-H. and Mardon, J.-P., " Microstructural Stability of M5 Alloy Irradiated up to High Neutron Fluences", *ZR-ASTM-STP1467*, 2006, pp. 175-204.

[11] Yueh, H. K., Comstock, R. J., Shah, H. H., Colburn, D. J., Dahlback, M. and Hallstadius, L., "Improved ZIRLO™ Cladding Performance through Chemistry and Process Modifications", *ASTM-STP1467*, 2006, pp. 330-348.

[12] Okamoto H., "Sn-Zr (Tin-Zirconium)", *J. Phase Equilibria and Diffusion*, Vol. 31, 2010, pp. 411-412.

[13] Carpenter, G. J. C., Ibrahim, E.F., and Watters, J.F., "The aging response of zirconium-tin alloys", *J. Nucl. Mater.,* Vol. 102, 1981, pp. 280-291.

[14] Charquet, D., Hahn, R Ortlieb, E Gros, J-P Wadier, J-F, "Solubility Limits and Formation of Intermetallic Precipitates in ZrSnFeCr Alloys", ASTM-STP, STP1023-EB ,10.1520/STP1023-EB, 1989.

[15] Tenckhoff, E., "Review of deformation mechanisms, texture, and mechanical anisotropy in Zirconium and Zirconium base alloys", *J. ASTM Intl*, Vol. 2 (4) , 1998, pp. 199-224.

[16] McCabe, R. J., Cerreta, E. K., Misra, A., Kaschner, G. C. and Tomé, C. N., "Effects of texture, temperature and strain on the deformation modes of Zirconium", *Phil. Mag.*, Vol. 86, 2006, pp. 3595-3611.

[17] Akhtar, A., "Basal slip in Zirconium," *Acta Metall.*, Vol. 21, 1973, pp. 1–11.

[18] Akhtar, A., "Compression of Zirconium single crystals parallel to the c-axis," *J. Nucl. Mater.*, Vol. 47, 1973, pp. 79–86.

[19] Akhtar, A., "Prismatic slip in Zirconium single crystals at elevated temperatures," *Met. Trans. A*, Vol. 6, 1975, pp. 1217-1222.

[20] Abdolvand, H. and Daymond, M. R., "Internal strain and texture development during twinning: Comparing neutron diffraction measurements with crystal plasticity finite-element approaches", *Acta Mater.,* Vol. 60 (5), 2012, pp. 2240-2248.

[21] Abdolvand, H., Daymond, M.R. and Mareau, C., "Incorporation of twinning into a crystal plasticity finite element model: Evolution of lattice strains and texture in Zircaloy-2", *Intl. J. Plasticity*, Vol. 27(11), 2011, pp. 1721-1738.

[22] Wang, J., Beyerlein, I. J., Hirth, J. P. and Tome, C. N. , "Twinning dislocations on {1011} and {1013} planes in hexagonal close-packed crystals", *Acta Mater.*, Vol. 59, 2011, pp. 3990–4001.

[23] Christian, J. W. and and Mahajan, S., "Deformation Twinning", *Prog. in Mater. Sci.*, Vol. 39, 1995, pp. 1-157.

[24] Jones, I.P. and Hutchinson, W.B. "Stress-state dependence of slip in Titanium-6Al-4V and other H.C.P. metals", *Acta Metall.*, Vol. 29 (6), 1981, pp. 951-968.

[25] Cai, S., Daymond, M. R. and Holt, R. A., "Deformation of high β-phase fraction Zr-Nb alloys at room temperature", *Acta Mater.*, Vol. 60(8), 2012, pp. 3355-3369.

[26] Garlea, E., Clausen, B., Kenik, E. A., Ciurchea, D., Vogel, S. C., Pang, J. W. L. and Choo, H., "Intergranular strain evolution in a zircaloy-4 alloy with basketweave morphology", *Metall. Materi. Trans. A: Physical Metallurgy and Materials Science*, Vol. 41(5), 2010 pp. 1255-1260.

[27] Mosbrucker, P., Daymond, M. R. and Holt, R. A., "In situ studies of variant selection during the α-β-α phase transformation in Zr-2.5Nb", *J. ASTM Intl.*, Vol. 8(1), 2011.

[28] Muránsky, O., Daymond, M. R., Bhattacharyya, D., Zanellato, O., Vogel, S. C. and Edwards, L. , "Load partitioning and evidence of deformation twinning in dual-phase fine-grained Zr-2.5%Nb alloy", *Mater. Sci. Engg. A*, Vol. 564, 2013, pp. 548-558.

[29] Pang, J. W. L., Holden, T. M., Turner, P. A. and Mason, T. E., "Intergranular stresses in Zircaloy-2 with rod texture", *Acta Mater.*, Vol. 47(2), 1999, pp. 373-383.

[30] Xu, F., Holt, R. A., Daymond, M. R., Rogge, R. B. and Oliver, E. C, "Development of internal strains in textured Zircaloy-2 during uni-axial deformation", *Mater. Sci. Engg. A*, Vol. 488, 2008, pp. 172-185.

[31] Rangaswamy, P., Bourke, M. A. M., Brown, D. W., Kaschner, G. C., Rogge, R. B., Stout, M. G. and Tomé, C.N., "A study of twinning in zirconium using neutron diffraction and polycrystalline modeling", *Metall. Mater. Trans. A: Physical Metallurgy and Materials Science*, Vol. 33, 2002, pp. 757-763.

[32] Allen, V. M., Da Fonseca, J. Q., Preuss, M., Robson, J. D., Daymond, M. and Comstock, R. J., "Determination and interpretation of texture evolution during deformation of a Zirconium alloy", *ASTM STP 1505*, 2009, pp. 550-563

[33] Holt, R. A., Daymond, M. R., Xu, F. and Cai, S., "Intergranual and interphase constraints in

Zirconium alloys", ASTM-STP, Vol. 5(6), 2008, pp. 776-795.

[34] Santisteban, J. R., Daymond, M. R., James, J. A. and Edwards, L., "ENGIN-X: A third-generation neutron strain scanner", *J Appl Crystallography*, Vol. 39(6), 2006, pp. 812-825.

[35] Daymond, M. R. and Priesmeyer, H. G., "Elastoplastic deformation of ferritic steel and cementite studied by neutron diffraction and self-consistent modelling ", *Acta Mater.*, Vol. 50(6), 2002, pp. 1613-1626.

[36] Grant, B. M. B., Francis, E. M., Quinta Da Fonseca, J., Daymond, M. R. and Preuss, M., "Deformation behaviour of an advanced nickel-based superalloy studied by neutron diffraction and electron microscopy ", *Acta Mater.*, Vol. 60, 2012, pp. 6829-6841

[37] MacEwen, S. R., Tome, C. and Faber J., "Residual stresses in annealed Zircaloy", *Acta Metall*. Vol. 37, 1989, pp. 979-989.

[38] Mac Ewen, S. R. and Tome, C., "Residual Stresses in Textured Zirconium Alloys", *Zr-ASTM-STP-28148S*, 1987, DOI: 10.1520/STP28148S.

[39] Douglas, D. L., "Metallurgy of Zirconium", Atomic Energy Rev, Vol.1, 1963.

[40] Kearns, J., "Thermal expansion and prefereed orientation in zircaloy", Bettice Atomic Power Laboratory, Report WAPD-TM-472, 1965.

[41] Trojanov, Z., Lukfi, P., Kral, F. and Kral, R., "Discontinuous low temperature deformation of Zr-Sn alloys", *Mater. Sci. Engg. A*, Vol. 137, 1991, pp. 151–155.

[42] A. Dlouh, Z. Trojanovfi, P. Lukfic, , "Thermally (non-)activated deformation of Zr-Sn Polycrystals", *Czech. J. Phys. B,* Vol. 38, 1998, pp. 482-484.

Figures and Tables

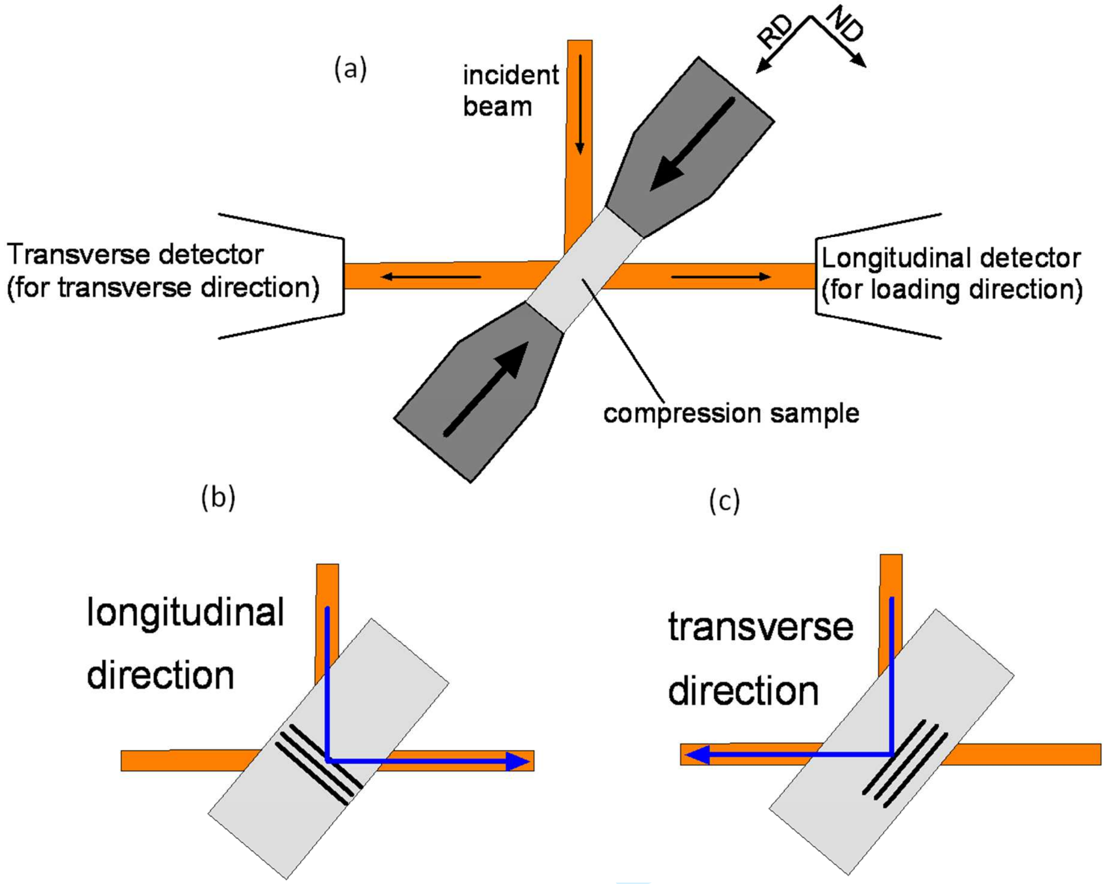

Fig. 1: Schematic illustrating (a) in-situ neutron diffraction experimental set up. (b) and (c) show the orientation of the crystallographic planes sensed by the two neutron detectors that are mounted on either side of the incident beam. Essentially, crystallographic planes of the sample, because of diffraction, act like mirrors to the incident neutron beam and deflect the incident beam on to the detectors. Depending on the location of the detectors, the response of either plane can be captured in the longitudinal (b) and transverse (c) direction in respect to the loading direction. RD and ND in (a) indicate the orientation of the sample's "Rolling" and "Normal" directions, as used in the present study.

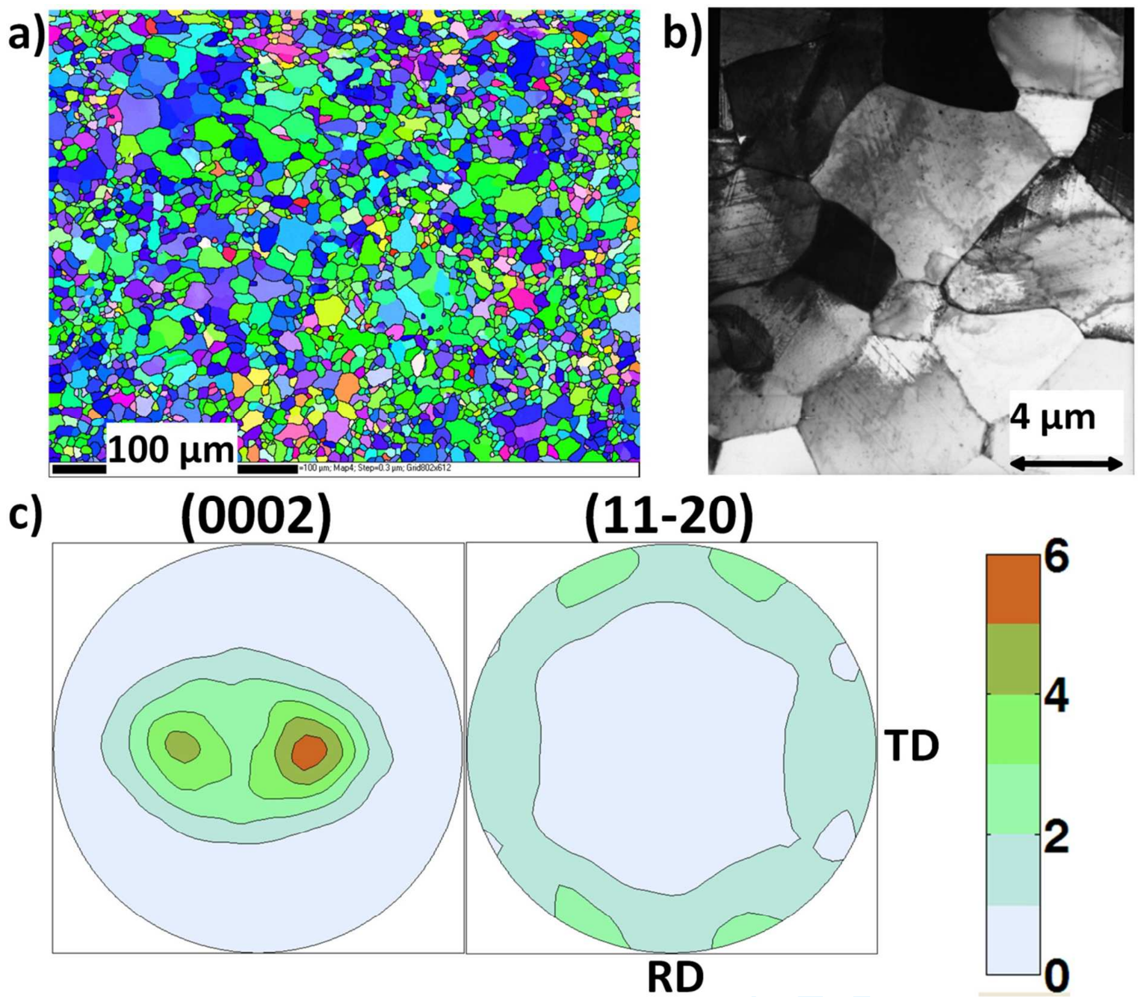

Fig. 2: Typical starting microstructure, a) EBSD and b) TEM, and (c) texture of the samples subjected to in-situ loading in neutron diffraction studies. In the present case the results were recorded on the Zr-1.2% Sn alloy.

.

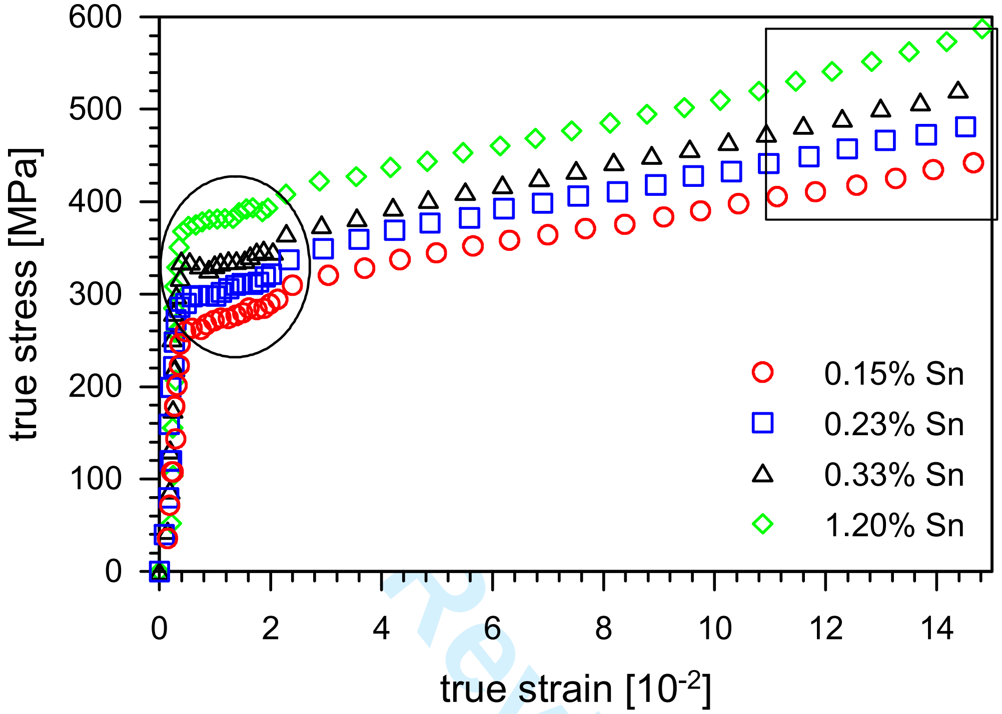

Fig. 3: Macroscopic true stress – true strain curves recorded during the in-situ compression/diffraction experiments. Circled region near the lower strain values indicates region of relatively low strain hardening. Regions highlighted by rectangular box exhibit increasing strain hardening rate with increasing Sn content.

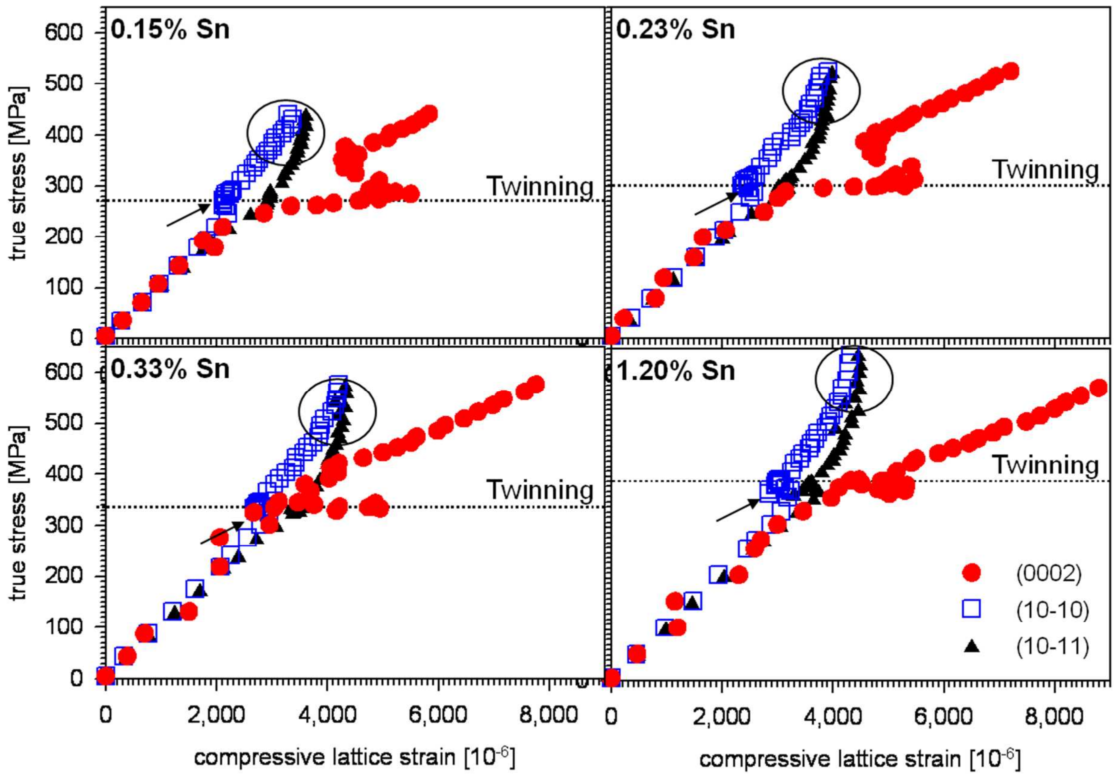

Fig. 4: Evolution of elastic lattice strains, along the loading direction, for the three families of orientations (0002, $10\bar{1}0$ and $10\bar{1}1$) during in situ compressive loading and neutron diffraction experiment for all the four Zr-Sn alloys used in the present study. The horizontal dotted lines in the plots represent the macroscopic applied stress at which onset of twinning was observed. Circled regions highlight the fact that with increasing Sn content, the differences between the $10\bar{1}0$ and $10\bar{1}1$ responses (i.e., separation of the respective curves) decreases. Increased extent of unloading of the $10\bar{1}0$ family of grains with increasing Sn content can also be observed (marked with the arrows).

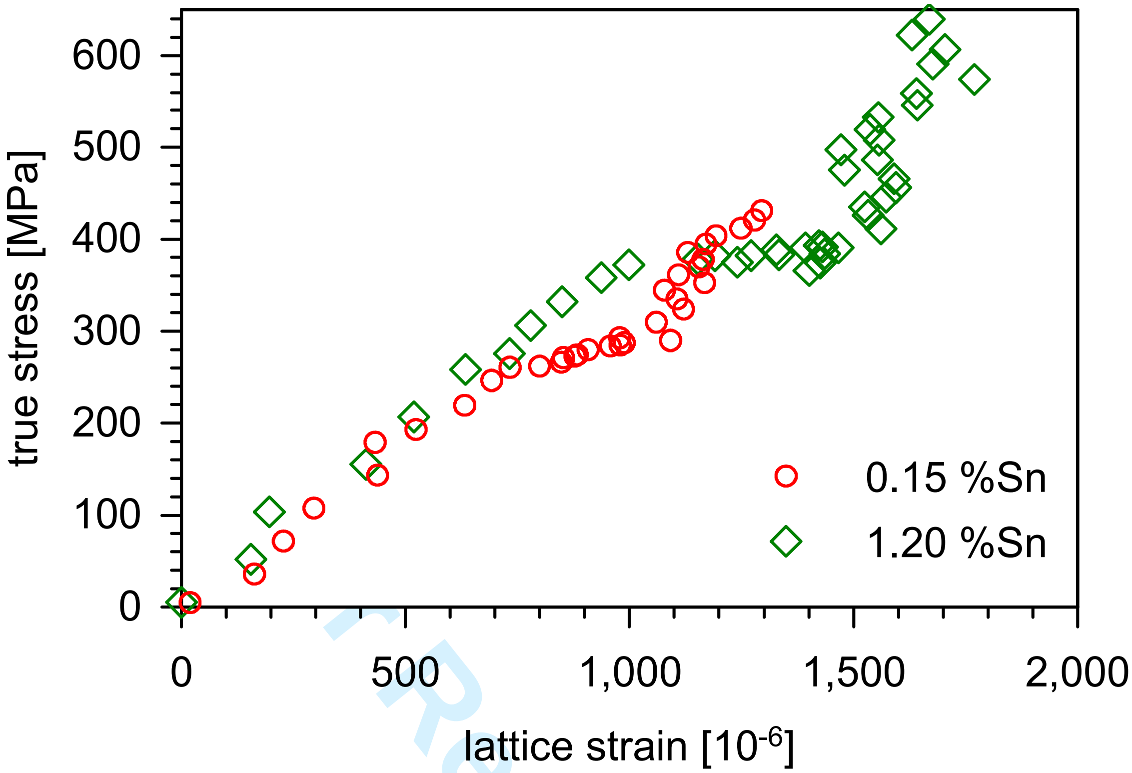

Fig. 5: Evolution of the (0002) lattice strains perpendicular to the loading (normal) direction during in situ compression loading and neutron diffraction experiment for Zr-0.15Sn and Zr-1.2Sn. The behaviour of the other two alloys is intermediate to these two extremes.

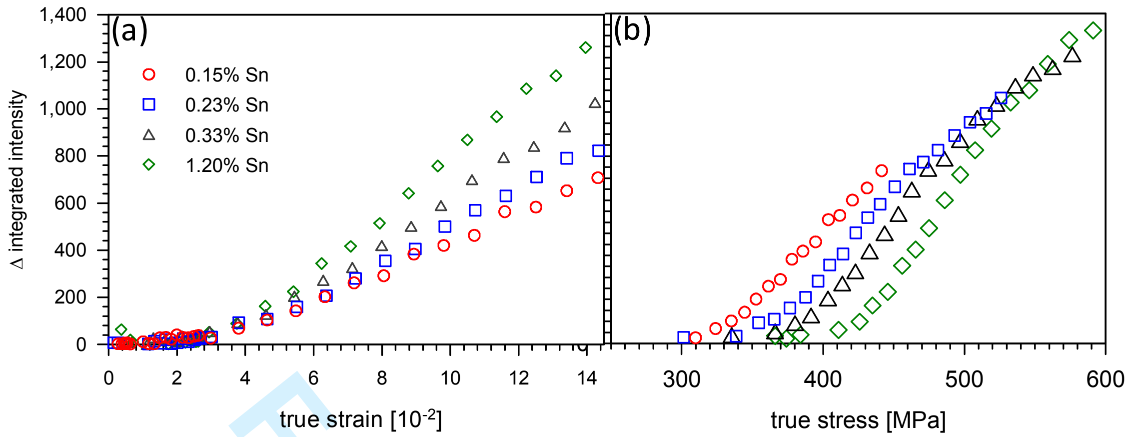

Fig.6: Change in the integrated intensity of the 0002 reflection recorded using detector along loading direction as a function of (a) true macroscopic strain (b) true macroscopic applied stress.

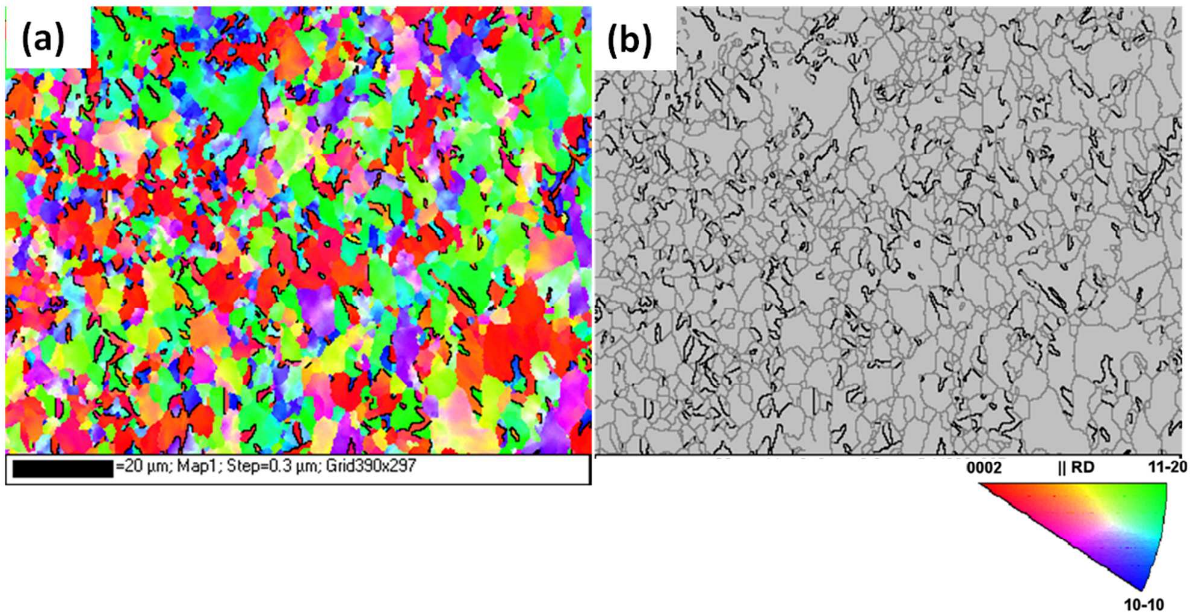

Fig.7: Zr-1.2%Sn deformed to 0.18 true strain (a) grain orientation map recorded by EBSD (IPF colour code) and (b) grain boundary map with high angle grain boundaries in grey and $\{10\bar{1}2\}\langle 10\bar{1}1\rangle$ twin boundaries in black.

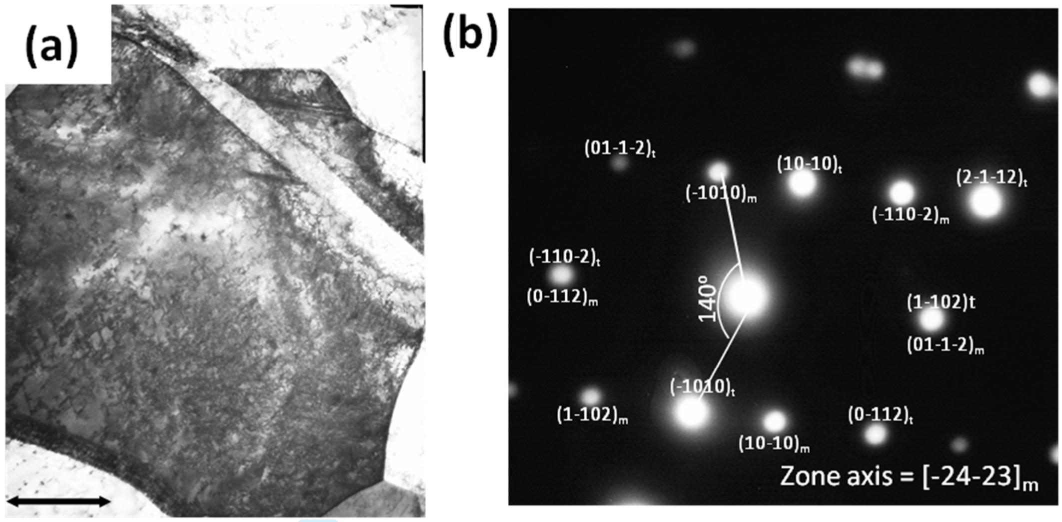

Fig. 8: TEM analysis with (a) bright field micrograph showing the formation of a twin in the early stage of deformation. The image is from a sample subjected to only 3% compressive deformation, and (b) composite diffraction pattern from the twin and matrix region recorded along $[\bar{2}4\bar{2}3]$ zone axis of the matrix grain. Misorientation between the matrix and twin is $140^o@[\bar{2}4\bar{2}3]$ which is symmetrically equivalent to $85^o@[2\bar{1}\bar{1}0]$ tensile twins.

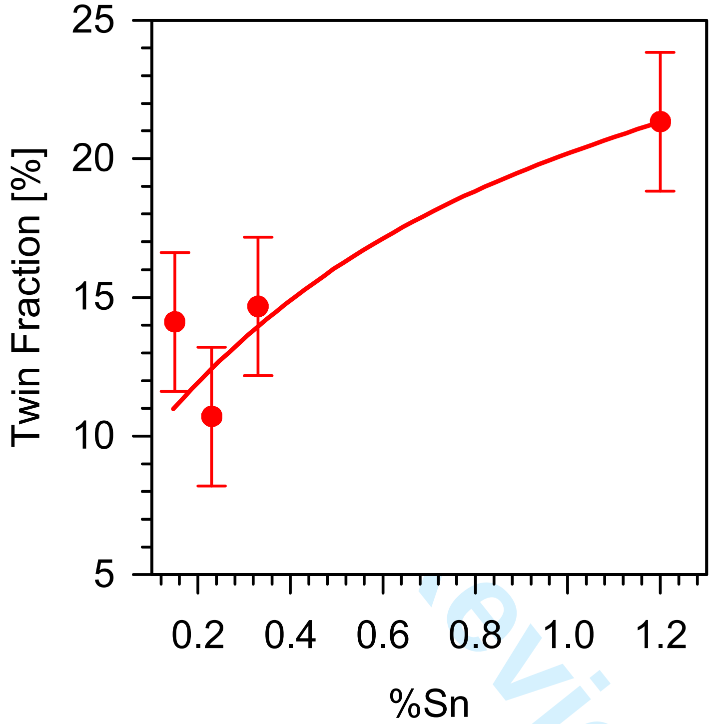

Fig. 9: EBSD derived twin volume fraction as a function of Sn content for the samples compressed to a strain of 0.18.

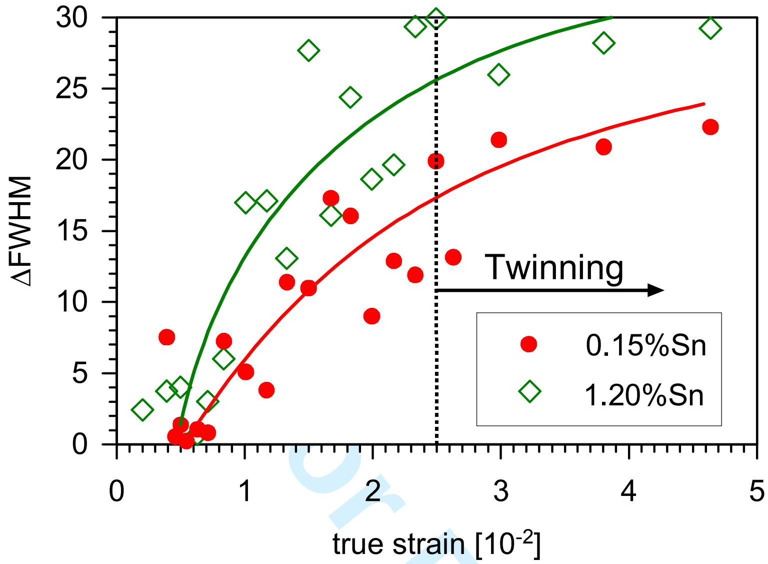

Fig. 10: Variation in FWHM of $11\bar{2}0$ peak (recorded along the loading direction) as a function of the strain for two of the alloys considered in the present study.

Tables

Table 1: Summary of the role of Sn on the yield stress, critical stress, and strains for the onset of twins.

Alloy Sn content (Wt%)	**0.15**	**0.23**	**0.33**	**1.2**
Macroscopic yield point (MPa)	260	281	303	352
Critical lattice strain for twin nucleation (10^{-6})	1050	1150	1350	1550
Critical plastic strain for twin nucleation (%)	1.3	1.5	1.6	2.1
Critical applied stress for twin nucleation (MPa)	271	300	356	391